

A Mixed Valence Copper Cyanide 3D-supramolecular Coordination Polymer Containing 1,10-Phenanthroline Ligand as a Potential Antitumor Agent, Effective Catalyst and Luminescent Material

Safaa El-din H. Etaiw · Said A. Amer ·
Mohamed M. El-Bendary

Received: 26 May 2011 / Accepted: 2 July 2011 / Published online: 17 July 2011
© Springer Science+Business Media, LLC 2011

Abstract The structure of the 3D-supramolecular coordination polymer (SCP) ∞ $\{[\text{Cu}^{\text{I}}(\text{CN})\cdot 2(\text{phen})\cdot \text{Cu}^{\text{II}}(\text{CN})_2\cdot (\text{phen})\cdot 5\text{H}_2\text{O}]\}$, **1** contains the $[\text{Cu}^{\text{I}}(\text{CN})\cdot 2(\text{phen})]$, $[\text{Cu}^{\text{II}}(\text{CN})_2\cdot (\text{phen})]$ molecular complexes and five water molecules which are connected with each other by hydrogen bonds. The most intriguing feature in the structure of **1** is the unusual supramolecular interactions, including hydrogen bonds which involve the terminal cyanide and the phenanthroline (phen) ligands and π – π stacking which generate a unique 3D-supramolecular architecture in the solid state. The emission spectrum of **1** displays a band centered at 420 nm which was assigned to S_0 –T transition in the CuCN fragments. This band suffers a shift to longer wavelength by about 30 nm than that of CuCN itself. The emission bands at 435, 450, and 475 correspond to the close lying π – π^* transitions of the coordinated phen. The main band at 435 nm exhibits a red shift than that of phen by about 70 nm which makes it attractive as luminescent sensor. Also, the **SCP 1** was used as heterogeneous catalyst for the degradation of Metanil Yellow (MY) dye by dilute solution of hydrogen peroxide as oxidant. The reaction is first order with respect to the MY dye. The 3-(4,5-dimethylthiazol-2-yl)-2,5-diphenyltetrazolium bromide (MTT) assay was used to determine the in vitro antitumor activity of the **SCP 1** on human breast cancer cell line, MCF7. The cytotoxicity of the **SCP 1** is more efficient than that of the Doxorubicin (DOX) drug. The thermal stability has been also investigated.

Keywords Mixed valence copper cyanide · Supramolecular coordination polymer · 1,10-Phenanthroline · Luminescence · Catalytic activity · Cytotoxicity

1 Introduction

Rational design and construction of cyanide-containing coordination polymers is becoming an increasingly popular field of research owing to their intriguing molecular topologies as well as exciting properties, such as, magneto-optics/electronics, catalysis, molecular sieving, ion exchange, luminescence, nano-particles, gas storage, and antitumor activity [1–5]. Transition metal cyanides have been studied extensively over the past two decades due to their great importance in magnetism and other properties [6, 7], but recent work focuses on copper(I) cyanide system because of the known versatility of $[\text{Cu}(\text{CN})]_n$ structural motifs in accommodating various ligands, and Cu(I) compounds have rich fluorescent properties [8–12]. Copper(I) cyanide coordination polymers incorporating diamine, organodiimine and N-heterocyclic ligands have been investigated by many authors [13–17]. It is worthy to note that mixed valence $\text{Cu}^{\text{II}}/\text{Cu}^{\text{I}}$ cyanide compounds have been rarely reported so far [13, 18, 19]. Thus, enormous efforts are being made in synthesizing, characterizing copper cyanides and exploring their functional properties.

On the other hand, phen has been extensively used for decades as a chemically versatile module exhibiting a fortunate combination of structural and chemical properties [20]. Its rigidity makes it an entropically better chelating molecule than the more common 2,2'-bipyridine and has been exploited to make a variety of simple geometrically diverse mononuclear complexes. In more recent times, taking advantage of the so-called template effect, phen

S. E. H. Etaiw (✉) · S. A. Amer · M. M. El-Bendary
Chemistry Department, Faculty of Science,
Tanta University, Tanta, Egypt
e-mail: safaaetaiw@hotmail.com

derivatives enabled the development of sophisticated synthetic strategies that have yielded fascinating molecular architectures such as catenanes, rotaxanes and knots [21]. Notably, some of these systems can be tailored to work as molecular-level machines [22]. Another important property of phen is connected to its planar structure, which prompts intercalation or groove binding with DNA or RNA [23]. In some cases phen derivatives are also used in optoelectronic devices, a classical example being bathocuproine (2,9-dimethyl-4,7-diphenyl-1,10-phenanthroline) which is employed as a hole blocking material to optimize the transport of electric charge in organic light emitting diodes (OLEDs) [20].

Supramolecular self-assembly was used to design copper cyanide mixed valence SCP containing phen, which has been carried out at room temperature between $[\text{Cu}(\text{CN})_4]^{3-}$ building blocks and phen. Thus, this work describes synthesis, crystal structure and antitumor activity of the SCP $\{[\text{Cu}^{\text{I}}(\text{CN})\cdot 2(\text{phen})\cdot \text{Cu}^{\text{II}}(\text{CN})_2\cdot (\text{phen})]\cdot 5\text{H}_2\text{O}\}$, **1**. The catalytic behavior of the **SCP 1** was tested for the degradation of azo-dyes (MY) by dilute solution of hydrogen peroxide as oxidant. Also, among the various aspects of chemical sciences concerned with phen, we focus on its versatility to afford a luminescent material at room temperature. Curiously, unmodified phen is a weakly emissive compound, but on complexation with copper a highly luminescent complex should be obtained to be used as luminescent probe.

2 Experimental

2.1 Materials and Physical Measurements

All chemicals and solvents used in this study were of analytical grade supplied by Aldrich or Merck and used as received except $\text{K}_3[\text{Cu}(\text{CN})_4]$, which was prepared in the laboratory according to literature [24]. MY dye (98% purity) was received from B.D.H. Chemicals Ltd and used as received. Microanalyses (C, H, N) were carried out with a Perkin Elmer 2400 automatic elemental analyzer. The IR spectra were recorded on Perkin Elmer 1430 Ratio Recording Infrared Spectrophotometer as KBr discs. The magnetic susceptibility was determined with Johnson-Matthey susceptometer. Thermogravimetric analysis was carried out on a Shimadzu AT 50 thermal analyzer (under N_2 atmosphere). Electronic absorption spectra as solid matrices and in DMF were measured on Shimadzu (UV-3101 PC) spectrometer. It was used to monitor the changes of the dye absorbance during the reaction course. Calibration plots based on Beer-Lambert's law relating the absorbance to the concentration were established at its maximum absorbance wavelength, λ_{max} , of 435 nm.

Fluorescent spectra as solid matrices were measured with a Perkin Elmer (LS 50 B) spectrometer.

2.2 Synthesis of $\{[\text{Cu}^{\text{I}}(\text{CN})\cdot 2(\text{phen})\cdot \text{Cu}^{\text{II}}(\text{CN})_2\cdot (\text{phen})]\cdot 5\text{H}_2\text{O}\}$, **1**

At room temperature, a solution of 99 mg (0.33 mmol) of $\text{K}_3[\text{Cu}(\text{CN})_4]$ in 30 mL H_2O was added, under gentle stirring to a solution of 60 mg (0.334 mmol) of 1,10-phenanthroline (phen) in 20 mL acetonitrile. After 1 week green needle crystals were resulted from yellow solution, after filtration, subsequent washing with water and overnight drying, about 70 mg (51% referred to $\text{K}_3[\text{Cu}(\text{CN})_4]$) of green crystals were obtained. $\mu_{\text{eff.}} = 1.95$ BM, Anal. Calc. for **1** ($\text{C}_{39}\text{H}_{34}\text{N}_9\text{O}_5\text{Cu}_2$): C, 56.0; H, 2.8; N, 15.0%. Found: C, 55.96; H, 2.7; N, 14.9%.

2.3 Catalytic Activity Measurements

For the catalytic runs a stock solution of the MY dye (5×10^{-5} M) was prepared in doubly distilled water. A number of reactors (100 mL) containing a definite quantity of the catalyst, **SCP 1** (0.025 mmol) together with the appropriate volume (3 mL) of the MY dye solution (5×10^{-5} M) were placed in a water shaker thermostat at 25 °C to attain this temperature. To each reactor 1 mL of 0.5 M H_2O_2 solution was added and the time was noted. After 2 min, aliquot of each flask was withdrawn and the absorbance was recorded. Also, at regular time intervals aliquot of each conical was withdrawn, filtrated to remove the catalyst, and the absorbance was recorded at λ_{max} of 435 nm. Generally, the dye/ H_2O_2 mixture was stable for several hours without changes in the absorbance. This means that no reaction takes place between the MY dye and H_2O_2 in the absence of the catalyst, **SCP 1**.

2.4 In vitro Antitumor Activity

In vitro potential cytotoxicity of the compounds was tested using the colorimetric method. The **SCP 1** dissolved in dimethylsulfoxide (DMSO) was subjected to cytotoxic evaluation against human breast adenocarcinoma cell line (MCF7). 3-(4,5-dimethylthiazol-2-yl)-2,5-diphenyltetrazolium bromide was dissolved in saline to make a concentration of 5 mg/mL as a stock solution. Cancer cells (5×10^5 cells) suspended in 200 μL of MEM medium containing 10% fetal calf serum were seeded onto a 96-well culture plate. After 24 h of preincubation at 37 °C in a humidified atmosphere of 5% CO_2 to allow cell attachment, various concentrations of the test solution were added and then incubated for 72 h under the above conditions. At the end of the incubation, 50 μL of tetrazolium reagent was added to each well and then incubated at 37 °C

for 4 h. The supernatant was decanted, and DMSO (100 μ L) was added to allow Formosan solubilization. The optical density (OD) of each well was detected by ELIZA microplate reader (Meter tech. Σ 960, U.S.A.) at 564 nm. Each determination represents the mean of four replicates. The 50% inhibition concentration (IC₅₀) was determined by curve fitting.

2.5 Crystal Structure Determination

Structural measurements for **1** were performed on a Kappa CCD Enraf–Nonius FR 90 four circle goniometer with graphite monochromatic MoK α radiation $\{[\lambda\text{Mo-K}\alpha] = 0.71073 \text{ \AA}\}$ at $25 \pm 2 \text{ }^\circ\text{C}$. The structure was solved using direct-methods and all of the non-hydrogen atoms were located from the initial solution or from subsequent electron density difference maps during the initial stages of the refinement. After locating all of the non-hydrogen atoms in each structure the models were refined against F^2 , first using isotropic and finally using anisotropic thermal displacement parameters. The positions of the hydrogen atoms were then calculated and refined isotropically, and the final cycle of refinements was performed.

3 Results and Discussion

In continue of our study on structure variability and flexibility associated with the study of the organometallic systems [5, 8–10], the reaction of the ternary adducts $\text{K}_3[\text{Cu}(\text{CN})_4]$, Me_3SnCl and phen was carried out in H_2O /acetonitrile medium at room temperature to obtain a bimetallic 3D-supramolecular coordination polymer. Unexpectedly, the organotin free mixed valence coordination polymer $\{[\text{Cu}^{\text{I}}(\text{CN}) \cdot 2(\text{phen}) \cdot \text{Cu}^{\text{II}}(\text{CN})_2 \cdot (\text{phen})] \cdot 5\text{H}_2\text{O}\}$, **1** was obtained. Also, the SCP **1** was directly obtained as green needle crystals by direct addition of $\text{K}_3[\text{Cu}(\text{CN})_4]$ and phen in H_2O /acetonitrile solution at room temperature in ca 51% yield. On the other hand, cyanobis(phen)copper(II)dicyano(phen)cuprate(1) hexahydrate, **1a**, was early prepared by adding a hot aqueous solution of 1,10-phenanthroline monohydrate and $\text{Cu}(\text{NO}_3)_2 \cdot 3\text{H}_2\text{O}$ to an aqueous solution of KCN. During the addition of KCN a more intense blue color formed with the subsequent precipitation of a non-crystalline substance. The hot mixture was quickly filtered and the green filtrate was transferred to a beaker, green needle like crystals which are light sensitive were isolated [25]. Later on, the reaction of 1 M $\text{Cu}(\text{NO}_3)_2$, 26% NH_3 and aqueous solution of 1,10-phenanthroline monohydrate which were mixed; on dropwise addition of 1 M aqueous solution of KCN, yielded a violet non-crystalline precipitate; the mixture was allowed to stand for 7 days at room temperature which formed well shaped

dark-green crystals of $\text{Cu}_2(\text{phen})_3(\text{CN})_3 \cdot 5\text{H}_2\text{O}$, **1b**. The crystals were unstable and cracked in air [26]. In the case of **1a** and **1b**, green crystals were recovered from an uncharacterized amorphous blue powder. In the present study, the green crystals of **1** were the only solid state product obtained at room temperature. Thus, the use of $\text{K}_3[\text{Cu}(\text{CN})_4]$ instead of $\text{Cu}(\text{NO}_3)_2$ affords the formation of green precipitate which is consisting exclusively of one discrete species and never of any mixture of different assemblies. The SCP **1** is light and air stable and insoluble in water but it is freely soluble in organic solvents.

3.1 Crystal Structure of the SCP 1

The empirical formula is $\text{C}_{39}\text{H}_{34}\text{Cu}_2\text{N}_9\text{O}_5$ which was supported by elemental analysis while the chemical composition $\{[\text{Cu}^{\text{I}}(\text{CN}) \cdot 2(\text{phen}) \cdot \text{Cu}^{\text{II}}(\text{CN})_2 \cdot (\text{phen})] \cdot 5\text{H}_2\text{O}\}$ of the SCP **1** was confirmed by single crystal X-ray study. The crystal data and the structure processing parameters of the SCP **1** are collected in Table 1. The asymmetric unit of the SCP **1** contains two discrete molecular structures and consists of two crystallography different Cu(I/II) atoms, three ordered cyanide groups, three phen molecules and five clathrated water molecules, Fig. 1.

The structure of the SCP **1** contains $[\text{Cu}^{\text{I}}(\text{CN}) \cdot 2(\text{phen})]$, $[\text{Cu}^{\text{II}}(\text{CN})_2 \cdot (\text{phen})]$ fragments and five water molecules which are connected with each other by hydrogen bonds. In $[\text{Cu}^{\text{I}}(\text{CN}) \cdot 2(\text{phen})]$ fragment, the copper center is

Table 1 Crystal data and processing parameters for the SCP **1**

Empirical formula	$\text{C}_{39}\text{H}_{34}\text{Cu}_2\text{N}_9\text{O}_5$
Formula weight g/mol	835.06
Temperature (K)	298
Crystal system	Triclinic
Space group	P1
a/ \AA	11.6581 (3)
b/ \AA	12.2318 (3)
c/ \AA	15.1757 (5)
$\alpha/^\circ$	105.9500 (14)
$\beta/^\circ$	102.8191 (14)
$\gamma/^\circ$	106.923 (2) $^\circ$
V/ \AA^3	1880.40 (9)
Z	2
$\mu(\text{Mo} - \text{K}\alpha)/\text{m.m}^{-1}$	1.17
Calculated density/ g cm^{-3}	1.197
Goodness-of-fit on F^2	1.996
$F(000)$	686
R indices [$I > 3\sigma(I)$] R1/wR2	0.042/0.077
R indices (all data)	0.079/0.087
R_{int}	0.040
Data/restraints/parameters	3273/0/496

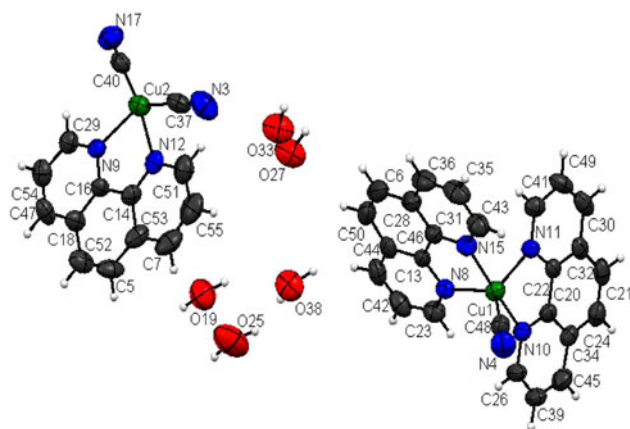


Fig. 1 An ORTEP plot of the asymmetric unit of the **SCP 1** with atom labeling scheme

coordinated by two phen ligands and one cyanide ligand in a distorted trigonal bipyramid (TBPY-5) geometry, $N8-Cu1-C48 = 123.68^\circ$, $N10-Cu1-C48 = 95.00^\circ$, $N15-Cu1-C48 = 93.23^\circ$, $N11-Cu1-N8 = 103.37^\circ$, Table 2. This deviation is due to the hydrogen bonds between the cyanide group and the water molecules, $N4-H27A = 3.10 \text{ \AA}$, $N4-H38B = 3.01 \text{ \AA}$, Table 3. It is interesting to observe that the dihedral angle between the planes defined by the copper and two nitrogen atoms of one phen ligand and by the copper and two nitrogen atoms of the other phen ligand is 76.74° . The N8, N11 and C48 atoms are present in equatorial positions while the N10 and N15 atoms occupy axial positions with nearly equivalent bond lengths; 2.01 \AA . Few examples of Cu^I , which form TBPY-5 geometry, are known [27, 28]. Recently, copper(I)/2,2'-bipyridine complexes were considered as the first class of trigonal pyramidal copper(I) complexes with p-coordinated electron poor olefins [29]. On the other hand, the copper

Table 2 Bond lengths (Å) and bond angles ($^\circ$) of the **SCP 1**

Cu1–N11	2.086 (2)	N10–Cu1–C48	95.00 (11)
Cu1–N10	2.014 (2)	N11–Cu1–C48	132.94 (11)
Cu1–C48	1.967 (2)	N8–Cu1–C48	123.68 (11)
Cu1–N15	2.011 (2)	N15–Cu1–C48	93.23 (11)
Cu1–N8	2.143 (2)	N11–Cu1–N8	103.37 (11)
Cu1–N10	2.014 (2)	N10–Cu1–N1	80.83 (11)
Cu2–C37	1.910 (3)	N8–Cu1–N15	80.04 (11)
Cu2–C40	1.929 (3)	N15–Cu1–C48	92.07 (11)
Cu2–N12	2.144 (3)	Cu1–C48–N4	176.74 (3)
Cu2–N9	2.142 (3)	N12–Cu2–N9	77.57 (11)
C48–N4	1.143 (3)	N12–Cu2–C37	100.59 (11)
C40–N17	1.128 (3)	N9–Cu2–C40	112.37 (11)
C37–N3	1.160 (3)	C40–Cu2–C37	130.26 (11)
		Cu2–C40–N17	176.97 (3)
		Cu2–C37–N3	172.18 (3)

Table 3 Hydrogen bond lengths (Å) and bond angles (deg.) in the **SCP 1**

D–H...A	d(D–H)	d(H...A)	d(D...A)	\angle (DHA)
O25–H25A...N17	0.960	2.830	2.770	76.94
O33–H33B...N3	0.960	2.947	2.739	58.33
O38–H38B...N4	0.960	3.011	2.931	76.04
O27–H27A...N4	0.960	3.107	2.830	64.54
O33–H33A...N3	0.960	3.118	2.947	58.33
C46–H46...O38	0.960	2.943	3.846	157.21
C50–H50...O27	0.959	3.014	3.915	156.98
C6–H6...O19	0.960	2.802	3.734	163.99
C55–H55...O27	0.960	2.757	3.698	166.6
C51–H51...O38	0.960	2.847	3.749	156.9
C7–H7...O25	0.959	3.062	3.889	145.34
C7–H7...O19	0.959	2.739	3.465	132.96
C55–H55...O19	0.960	3.277	3.727	110.76
C41–H41...C43	0.961	2.886	3.571	129.16
C23–H23...C26	0.960	2.939	3.641	130.93
C46–H46...C51	0.960	3.214	3.623	107.63
C51–H51...C46	0.960	3.288	3.623	102.72

atom, in the $[Cu^I(CN)_2(phen)]$ fragment, is coordinated to one phen ligand and two cyanide groups, forming slightly distorted tetrahedral (T-4) geometry, $N9-Cu2-C40 = 112.37^\circ$, $C40-Cu2-C37 = 130.26^\circ$, $N12-Cu2-N9 = 77.57^\circ$, $N12-Cu2-C37 = 100.59^\circ$. Among metal ions of biological importance, the copper(II) ion presents a high number of complexes with distortion. In blue copper proteins, Cu^{II} shows an elongated $C3v$ distorted tetrahedral stereochemistry [30]. Also, several complexes contain Cu^{II} tetrahedral geometry [31–35]. Tetrahedrality for any tetra coordinate complex can be characterized by the angle subtended by two planes, each encompassing the copper and two adjacent donor atoms. For strictly square-planar complexes with $D4h$ symmetry, the tetrahedrality is 0° . For tetrahedral complexes with $D2d$ symmetry, the tetrahedrality equals 90° . In **1** the angle of the two planes; $C17Cu2C40$ and $N12Cu2N9$, is 85.21° supporting the tetrahedral geometry of Cu^{II} . All the Cu–N bonds are in the range of the reported values [8–10, 13–17]. There are five clathrated water molecules per $[Cu^I(CN)_2(phen)] \cdot [Cu^{II}(CN)_2(phen)]$ fragments which form hydrogen bonds, Table 4. Further analysis of the crystal packing reveals that the oxygen atoms of the water molecules are close packed by short contacts in the range of 2.75 – 2.87 \AA , Table 5, forming a unique 1D-tape, Fig. 2a. This 1D-tape consists of fused two four- and one six-oxygen member rings creating water cluster. In addition the water molecules are connected via hydrogen bonds forming 1D-chain. These hydrogen bonds are formed between the oxygen atoms of the water molecules and hydrogen atoms of the other water molecules;

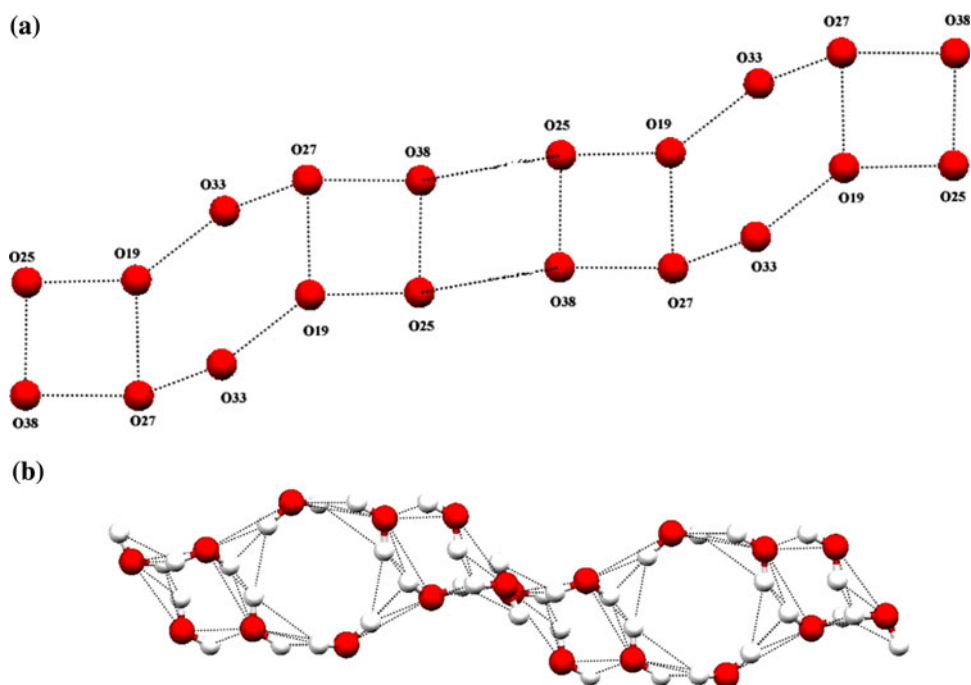
Table 4 Hydrogen bond lengths (Å) and bond angles (deg.) between water molecules in the **SCP 1**

D–H...A	d(D–H)	d(H...A)	d(D...A)	∠(DHA)
H19A–O19...H27B	0.959	2.041	2.851	140.95
H38B–O38...H25B	0.960	2.060	2.931	150.01
H27A–O27...H19B	0.960	2.111	2.642	113.25
H19A–O19...H25A	0.959	2.545	2.850	98.53
H19A–O19...H25B	0.959	2.818	3.525	131.20
H27B–O27...H38B	0.960	2.960	3.455	113.34
H25A–O25...H19B	0.960	3.143	3.094	78.27

Table 5 The distances (Å) of the π – π stacking and short contacts in the structure of the **SCP 1**

O4–O27	2.830	C41–C43	3.571
O27–O19	2.876	C45–C49	3.600
O27–O38	2.804	C46–C51	3.623
O25–O38	2.761	C23–C22	3.641
O19–O25	2.764	C21–C46	3.778
O25–O17	2.775	C30–C34	3.761
O33–O27	2.860	C55–C46	3.891
O38–N4	2.931		

(2.041–3.143 Å), Table 4, Fig. 2b. The water molecules spread between the layers of the $[\text{Cu}^{\text{I}}(\text{CN})_2 \cdot 2(\text{phen})]$ and $[\text{Cu}^{\text{II}}(\text{CN})_2 \cdot (\text{phen})]$ fragments forming H-bonds with the terminal cyanide groups and the hydrogen atoms of the phen ligand to extend the structure of **1** to 3D-network. So,

Fig. 2 **a** 1D-tape of the cluster water molecules. **b** 1D-tape of the clathrated water molecules connected by H-bonds

these water tapes play a complementary role via hydrogen bonds for stabilizing the network structure of the **SCP 1** in addition to the π – π stacking, Fig. 3.

Cyanometallates are useful building blocks for the construction of supramolecular structures. Such supramolecular assemblies are usually achieved through bridging linear coordinate $\text{M}–\text{CN}–\text{M}$ bonding interactions [36]. In contrast successful attempts to use cyanide as a terminal ligand, especially as a hydrogen-bond acceptor, are rare [37, 38]. The most intriguing feature in the structure of the **SCP 1** is its unusual supramolecular interactions, including $\text{H}\cdots\text{N}–\text{C}$ hydrogen bonds and π – π stacking to generate a unique 3D-supramolecular architecture in the solid state, Figs. 3 and 4 & Tables 3, 4, and 5. Alternatively, the 3D-network structure of **1**, down the projection of the *c*-axis, consists of fused six-member rings creating box-like structure. The $[\text{Cu}^{\text{II}}(\text{CN})_2 \cdot (\text{phen})]$ fragments occupy two facing sides of the hexagon while the other four sides consist of the terminal cyanide groups connected by the water molecules via H-bonds. Interestingly, the $[\text{Cu}^{\text{I}}(\text{CN})_2 \cdot 2(\text{phen})]$ fragments occupy the center of the hexagon while they are connected to the sides of the hexagon by H-bonds, Fig. 3. It is worth mentioned that there are no Cu–Cu interactions since the shortest distances between $\text{Cu}1–\text{Cu}2 = 6.137$ Å, $\text{Cu}1–\text{Cu}1 = 7.599$ Å, and $\text{Cu}2–\text{Cu}2 = 12.692$ Å.

Consulting the crystal structure of **1** and **1b** reveals that the crystal structure of **1b** was found to consist of discrete $[\text{Cu}^{\text{II}}(\text{phen})_2\text{CN}]^+$ cations and $[\text{Cu}^{\text{I}}(\text{phen})(\text{CN})_2]^-$ anions held together by hydrogen-bonded water molecules. The structure was also described as containing of dimeric

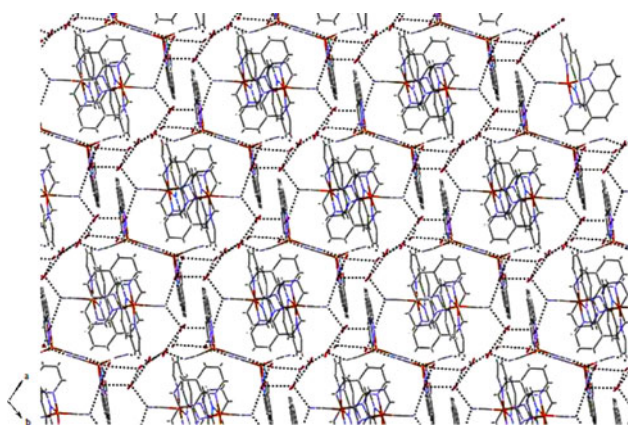


Fig. 3 3D-network structure showing hydrogen bonds in the SCP 1 along the *c*-axis

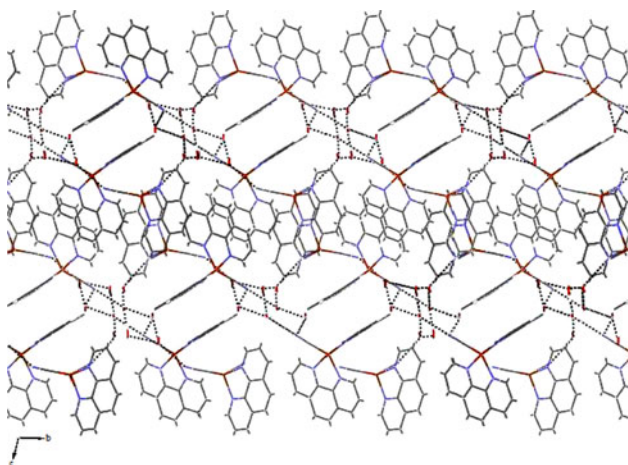


Fig. 4 3D-network structure showing hydrogen bonds in the SCP 1 along the *a*-axis

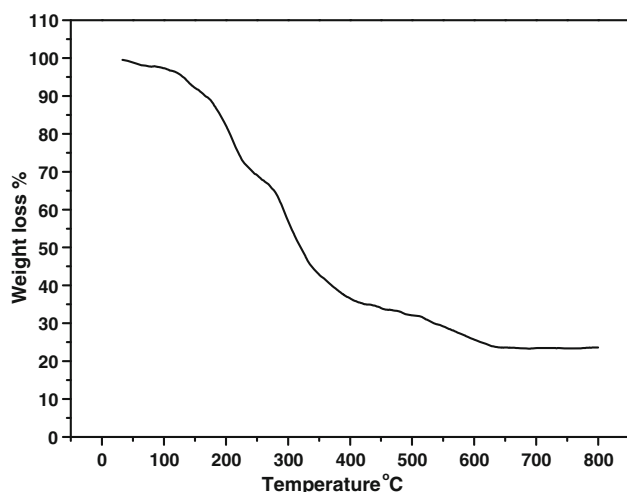


Fig. 5 Thermogravimetric analysis of the SCP 1

clusters of composition $\{[\text{Cu}^{\text{II}}(\text{phen})_2(\text{CN})][\text{Cu}^{\text{I}}(\text{phen})(\text{CN})_2(\text{H}_2\text{O})_5]\}_2$ [26]. On the other hand, the structure of **1** consists of discrete neutral molecules with separation distances which largely exceed the distance of an ionic bond. The shortest distance between any two close Cu^{I} and Cu^{II} atoms is 6.137 Å while the distances between the two CN ligands of the $[\text{Cu}^{\text{II}}(\text{phen})(\text{CN})_2]$ complex and the Cu atom of the $[\text{Cu}^{\text{I}}(\text{phen})_2\text{CN}]$ complex are $\text{N}3\text{--Cu}1 = 5.803$ Å and $\text{N}17\text{--Cu}1 = 5.625$ Å, the case which excludes any ionic interaction. Also, **1** is water insoluble while the ionic compounds should be water soluble. In addition, the water molecules play an essential role to connect these neutral complexes via extensive hydrogen bonds creating 3D-network.

3.2 Infrared Spectrum of the SCP 1

The high energy region of the IR spectrum of the SCP 1 exhibits a strong broad band at 3397 cm^{-1} corresponding to the stretching vibrations of the water molecules. The IR spectrum of the SCP 1 exhibits bands characteristic of the $(\text{CuCN})_n$ fragment and the phen ligand. The spectrum displays the bands of the phen ligand at $3059, 2926\text{ cm}^{-1}$ ($\nu_{\text{CH}(\text{arom})}$), 1421 cm^{-1} (δ_{CH}) and at $770, 724\text{ cm}^{-1}$ (γ_{CH}). These bands are shifted to lower wave numbers from the vibration frequencies of the free phen ligand due to the formation of hydrogen bonds between the hydrogen atoms of the ligand and the donor sites of the $(\text{CuCN})_n$ fragment [39]. In contrast, the band at 1617 cm^{-1} corresponds to $\nu_{\text{C}=\text{N}}$ while those at $1586, 1507$ and 1459 cm^{-1} are attributed to $\nu_{\text{C}=\text{C}}$ of the phen ligand in the SCP 1. These bands exhibit small shifts to lower wave numbers from those of the phen ligand supporting coordination of phen to Cu centers.

The presence of two $\nu_{\text{C}\equiv\text{N}}$ IR absorption bands in the spectrum of the SCP 1 at 2129 and 2086 cm^{-1} supports the presence of two different cyanide groups. The first type of the cyanide groups is bonded to Cu^{I} while the other is coordinated to Cu^{II} center, supporting the presence of mixed valence copper cyanide coordination polymer. It is noteworthy that the $\nu_{\text{C}\equiv\text{N}}$ bands ($2129, 2086\text{ cm}^{-1}$) of the SCP 1 are different from that of $\text{K}_3[\text{Cu}(\text{CN})_4]$ (2081 cm^{-1}), which also supports the presence of two types of cyanide groups. In addition, the $\nu_{\text{Cu}=\text{C}}$ bands at 429 and 435 cm^{-1} confirm the presence of two $(\text{CuCN})_n$ fragments.

3.3 Thermogravimetric Analysis

The thermogram of the SCP 1, Fig. 5 shows four degradation steps. The first step at $80\text{--}160^\circ\text{C}$ corresponds to the release of the five water molecules, $\Delta m\%$ obser. (calc.) 10.5 (10.7). The second step involves removal of one phen ligand at $160\text{--}250^\circ\text{C}$, $\Delta m\%$ obser. (calc.) 21.0 (21.5). The third step in the temperature range $250\text{--}500^\circ\text{C}$ is due to

the release of the other two phen ligands, $\Delta m\%$ obser. (calc.) 42.5 (43.1). At 500–650 °C the weight loss is due to the decomposition of the three cyanide groups, $\Delta m\%$ obser. (calc.) 9.0 (9.3). The molecular weight of the residue obtained after complete thermolysis of the **SCP 1**, under nitrogen atmosphere, is coincident with metallic copper, mass% obser. (calc.) 24.0 (23.5), Table 6.

The thermogravimetric analysis of the **SCP 1** indicates that the structure of the **SCP 1** contains stable Cu^{I} $^{\text{I}}\text{CN}$ chains up to 700 °C while the phen ligands evolve at relatively high temperatures indicating that the phen molecules are strongly tied in the 3D-network via hydrogen bonds and strong coordination to the copper atoms. Also, the starting release of the water molecules at 80 °C indicates that water molecules are not coordinated to the copper atoms. However, this temperature, which extends up to 160 °C for complete release of water molecules, indicates the formation of hydrogen bonds that need relatively high temperature to break down.

3.4 Spectroscopic Properties of the SCP 1

The electronic absorption spectrum of 1,10-phenanthroline resembles the spectra of phenanthrene and anthracene and consequently that of naphthalene. Substitution of nitrogen for methane in the 1,10-phenanthroline, just as in naphthalene, produces only relatively small spectroscopic changes, Table 7 and Fig. 6. The short wavelength band in phenanthroline, with a peak at 200 nm is assigned to the $^1\text{B}_a \leftarrow ^1\text{A}$ transition. The longitudinally polarized $^1\text{B}_b \leftarrow ^1\text{A}$ band at 225 nm resembles that observed in the spectrum of phenanthrene at 221 nm [40]. The broad band at 260 nm can be considered as a composite one, since the $^1\text{L}_b$ band was submerged under the $^1\text{L}_a$ band like the case in the anthracene [40]. This band exhibits blue shift than that observed in the spectra of naphthalene (286 nm) and anthracene (310 nm) [40]. Thus, this broad band can be assigned to $^1\text{L}_a \leftarrow ^1\text{A}$ and $^1\text{L}_b \leftarrow ^1\text{A}$ transitions. The last long wavelength band at 285 nm is weak and corresponds to $n \rightarrow \pi^*$ transition which disappears on the addition of HCl.

Table 6 Thermogravimetric analysis data of the **SCP 1**

Step	Temp. range (°C)	$\Delta m\%$ Obs.	$\Delta m\%$ Cal.	Assignment
1	80–160	–10.5	–10.7	–5(H_2O)
2	160–250	–21.0	–21.5	–(phen)
3	250–500	–42.5	–43.1	–2(phen)
4	500–650	–9.0	–9.3	–3(CN)
Residue	Temp. range (°C)	Mass _{obs} %	Mass _{cal} %	
3Cu %	Over 700	24.0	23.5	3Cu %

Table 7 Absorption and emission bands of **phen** and the **SCP 1**

Compound	λ_{abs} (nm)	Assignment	λ_{em} (nm)	Assignment
phen	198	$^1\text{B}_a \leftarrow ^1\text{A}$		Close laying $\pi \rightarrow \pi^*$ transition
	255	$^1\text{B}_b \leftarrow ^1\text{A}$	365	
	260 ^b	$^1\text{L}_a \leftarrow ^1\text{A}$	380	Triplet excimer of phen
	285	$^1\text{L}_b \leftarrow ^1\text{A}$	425	
		$n \rightarrow \pi^*$	555	
SCP 1	200	$^1\text{B}_a \leftarrow ^1\text{A}$	420	$\text{S}_0 \rightarrow \text{T}$ (CuCN) + MC
	225	$^1\text{B}_b \leftarrow ^1\text{A}$		
	265 ^b	$^1\text{L}_a \leftarrow ^1\text{A}$	435	Close laying
		$^1\text{L}_b \leftarrow ^1\text{A}$	450	$\pi \rightarrow \pi^*$ Transition
			475	MLCT

^b broad

On the other hand, the spectrum of the **SCP 1** displays the same bands of phenanthroline at more or less the same positions, Table 7 and Fig. 6, except that the $n \rightarrow \pi^*$ band disappears indicating the participation of phenanthroline in the coordination sphere of copper.

It is well known that the unmodified phen is a weakly emissive compound but, following several routes, a wide range of highly luminescent phenanthroline compounds with emission bands ranging from the UV to the near infrared region can be obtained [41]. Phenanthroline exhibits close laying $\pi \rightarrow \pi^*$ and $n \rightarrow \pi^*$ singlet excited states and the emission originates mainly from the former [20, 42]. $n \rightarrow \pi^*$ Excited states often decay via non-radiative pathways and they are usually characterized by vanishingly low emission quantum yields. Phenanthroline itself, is characterized by a weak fluorescence quantum yield ($\Phi_{\text{fl}} = 0.0087$) and a short singlet lifetime ($t < 1$ ns) at room temperature [41]. The emission spectrum of phen in DMF displays well developed peak at 365 nm, two

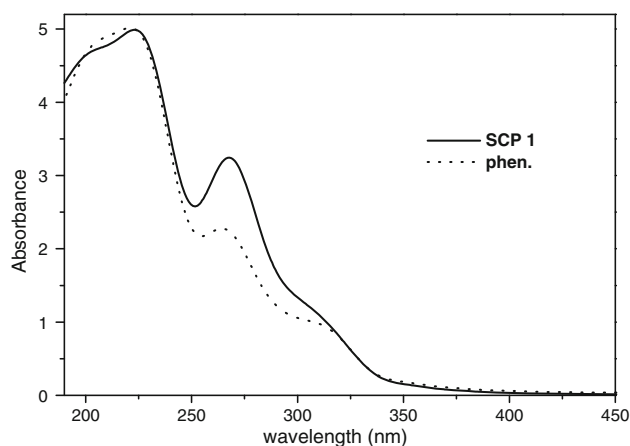


Fig. 6 Electronic absorption spectra of **phen** in DMF and the **SCP 1** in solid state

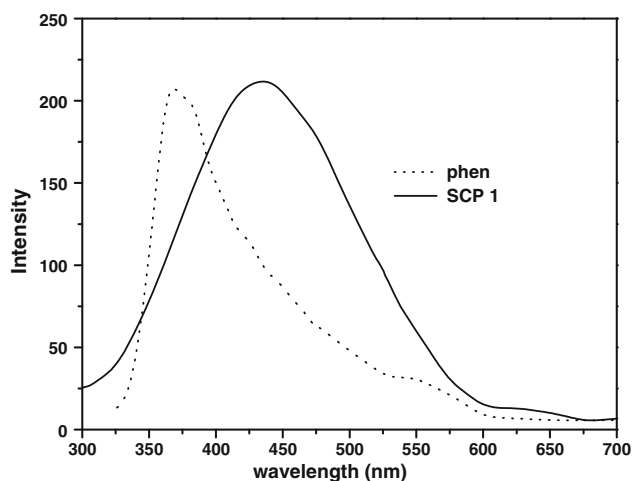


Fig. 7 Emission spectra ($\lambda_{ex} = 280$ nm) of **phen** in DMF and the **SCP 1** in solid state

shoulders at 380 and 425 nm and a very weak band at 555 nm, Table 7 and Fig. 7. The first three structured bands correspond to the close lying $\pi-\pi^*$ transition. The low-energy, delayed emission band at 555 nm can be assigned to the triplet excimer of phen as was supported by the concentration dependence of the delayed emission band. This assignment was also substantiated by reference to the excimer phosphorescence of naphthalene, quinoxaline and phenanthroline [43]. The experimental results regarding the combination dependence of delayed emission are favored to suggest that the emission at 555 nm is due to the excimer phosphorescence of phenanthroline.

With respect to the emission spectrum of the **SCP 1**, $\{[\text{Cu}^{\text{I}}(\text{CN})\cdot 2(\text{phen})\cdot \text{Cu}^{\text{II}}(\text{CN})_2\cdot (\text{phen})]\cdot 5\text{H}_2\text{O}\}$, it displays a broad band with shoulders at 420, 435, 450, and 475 nm. The structure of the **SCP 1** contains the CuCN fragment and the phen ligand, both of them luminescence at $\lambda_{\text{max}} = 392$ nm [44]. It was found that the amine-bearing CuCN complexes emit in the visible region while their photophysical behavior appears to be closely to that of CuCN itself [45]. The emission spectrum of CuCN is assumed to arise from transition between the lowest triplet excited state and the ground state. It is also, supposed that a bent triplet state is responsible for the relatively high energy CuCN emission [46]. On the other hand, the photophysical properties of phen, as well as, that of CuCN can be tuned by the formation of the SCP. The emission spectrum of the **SCP 1** exhibits a broad band centered at 420 nm. This band can be assigned to So–T transition in the CuCN fragments which suffers a shift to longer wavelength by about 30 nm than that of CuCN itself. The bands at 435, 450, and 475 correspond to the close lying $\pi-\pi^*$ transitions of the coordinated phen, Table 7 and Fig. 7. The main band at 435 nm exhibits a red shift than that of phen by about 70 nm moving from the UV-to the

visible region. Thus, the luminescence behavior of phen shows excellent sensitivity towards copper which makes it attractive as luminescent sensor. However, one can not ignore, due to the broadening of the bands, the possibility of single-metal-centered (MC) transitions of the type $3d^{10} \rightarrow 3d^9 4s^1$ and $3d^{10} \rightarrow 3d^9 4p^1$ on the Cu(I) center, (low energy bands) and the metal to ligand charge transfer (MLCT) (high energy band).

3.5 Catalytic Studies of the SCP 1

Wastewater from the textile industry contains significant concentrations of organic matter that contribute to the toxicity of the effluents. It is well known that the stability and high degree of aromaticity in azo dyes prevent mineralization of these compounds by conventional aerobic biological treatment processes. Thus, there is currently considerable interest in developing alternative techniques that can degrade organic pollutants and be more cost-effective and environmentally benign [47]. Between others, catalysis is a powerful tool for such propose and different kinds of processes have been developed, mainly for the oxidation of organic pollutants [48]. Hydrogen peroxide is widely used in almost all industrial areas, particularly in the chemical industry and environmental protection [49]. The only degradation product of its use is water, and thus it has played a large role in environmentally friendly methods in the chemical industry. The versatile topology of the **SCP 1**, as the structure contains $\text{Cu}^{\text{I}}/\text{Cu}^{\text{II}}$ sites with good separation distances between these copper sites, encourages investigating its activity as catalyst for the degradation of organic dyes.

When MY dye was added to hydrogen peroxide in the absence of the **SCP 1** catalyst no changes in the absorption spectrum have been observed indicating that H_2O_2 alone is unable to degrade the MY dye. The reaction was initiated when the **SCP 1** was added as catalyst. The final solution is completely bleached as illustrated by the absorption spectra of MY in water (at $\lambda_{\text{max}} = 435$ nm) at the beginning and end of the reaction. Figure 8 shows the absorbance of MY in water before and after the reaction with H_2O_2 in presence of the **SCP 1** as catalyst. After 30 min, there is a fast degradation of MY, about 95.1% of the MY dye is degraded. This is may be due to increase of the π -conjugation within the heterocyclic aromatic N-donors, which leads to greatly enhanced hydrolytic stability of the **SCP 1** which is a necessary condition for catalytic oxidation processes [50]. It is worth mentioned here that the components of the **SCP 1** ($[\text{K}_3(\text{Cu}(\text{CN})_4]$ and phen) have no catalytic activity towards the degradation of MY when they are tested at the same conditions. On the other hand, investigation of the catalyst after the catalytic cycle by elemental analysis and the different spectroscopic methods

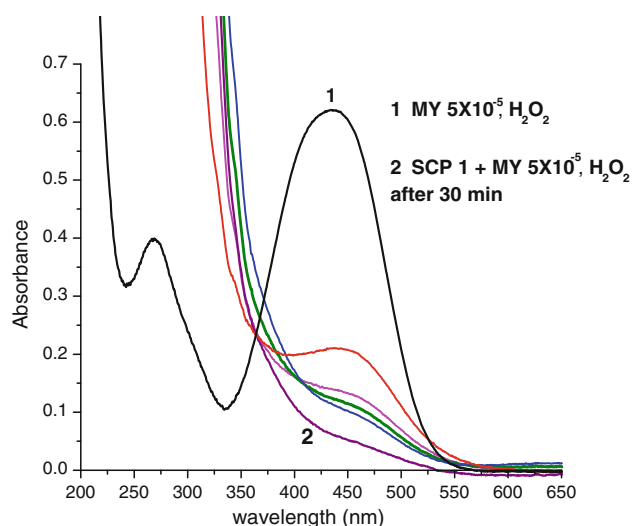


Fig. 8 The effect of time on the catalytic degradation of 5×10^{-5} M MY dye in the presence of 0.1 M H_2O_2 in absence and presence of 0.025 mmol of catalyst **1**

show that the catalyst is stable keeping its identity. Also, magnetic susceptibility measurements reveal that the used catalyst, **1** still paramagnetic ($\mu_{\text{eff.}} = 1.95$ BM), which indicates that the structure of the **SCP 1** catalyst after the catalytic cycles remains containing the Cu(I)/Cu(II)CN building blocks.

3.6 Kinetic Studies

Detailed kinetic study has been carried out on the catalytic activity of the **SCP 1**. When H_2O_2 solution was added to the MY dye solution in presence of the catalyst **1**, a dramatic decrease in the MY absorbance (at $\lambda_{\text{max}} = 435$ nm) with time was observed which indicates the degradation of the MY molecule. The degradation profile of the MY dye with initial concentration of $[\text{H}_2\text{O}_2]_0 = 0.1$ M and 0.025 mmol of the catalyst **1** is shown in Fig. 9. The kinetic study was carried out under pseudo-first order conditions with respect to the MY dye, where the initial concentration of hydrogen peroxide, $[\text{H}_2\text{O}_2]_0$, was at least 10-fold excess over $[\text{MY}]_0$. The observed rate constant, k_{obs} , was determined from the slope of the first-order plot, which verify Eq. 1.

$$\ln A_t = \ln A_0 - k_{\text{obs}}t \text{ or } \ln A_0/A_t = k_{\text{obs}}t \quad (1)$$

A_t is the absorbance at time = t and A_0 is the absorbance at $t = 0$.

The specific rate constant k was determined from the relation $k = k_{\text{obs}}/[\text{H}_2\text{O}_2]$ which equals to 1.2 L/mol min, ($R^2 = 0.978$). The spectral measurements show that about 100% of the MY dye was degraded completely into its mineral components after about 40 min.

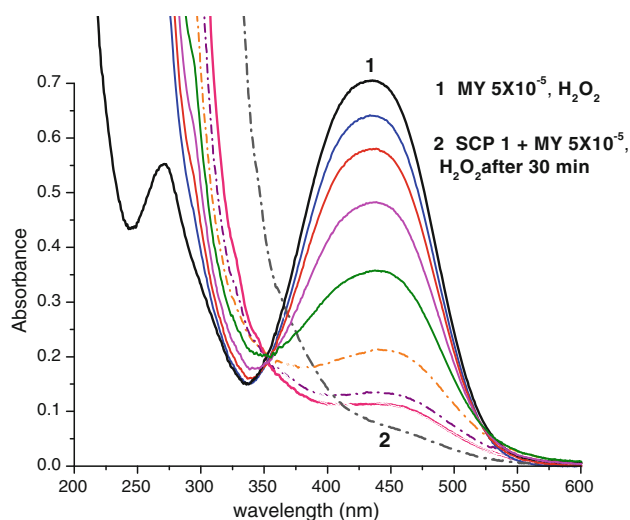
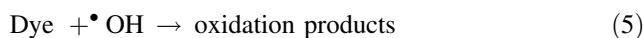
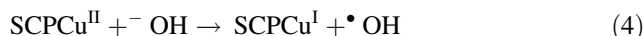


Fig. 9 Absorption spectra of MY dye 5×10^{-5} M in water in the beginning and every 2 min of the reaction with 0.1 M H_2O_2 in presence of 0.025 mmol of catalyst **1**

3.7 Mechanism

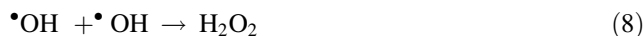
Based on the experimental findings and observations, the reaction mechanism has been suggested utilizing the redox properties of H_2O_2 . These properties involve a cyclic electron transfer process, which is initiated either by transfer of an electron from H_2O_2 to the oxidizing sites of the catalyst; Cu(II) to produce the HO_2 radical or transfer of an electron from the reduced sites of the catalyst; (CuI) to H_2O_2 to produce $\cdot\text{OH}$ [51, 52]. These radical species interact to give the degradation products. A reaction mechanism involving free radical species can be proposed as;



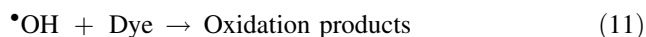
The hydroxyl radical propagates the reaction by reacting with the organic dye to produce further radicals, which can then react in many different steps.



Additionally, many other reactions are also possible, which include the radical–radical reaction or the reaction of the OH radical with H_2O_2 .



The other possibility is the transfer of an electron from H_2O_2 to the oxidizing sites of the catalyst; Cu(II) to produce the HO_2 radical



However, the actual mechanism needs further extensive experiments which are under current investigation. Also, the promising catalytic activity of the **SCP 1** for organic reactions should be the subject of further studies where its structure involves a copper(I) complex in conjunction with a C2-symmetric phen ligand [53].

3.8 In vitro Effects of the SCP 1 on MCF 7 Human Breast Cancer Cell Line Viability

Breast cancer is the most common invasive malignancy, and it is the invasive and metastatic of breast tumors that confound treatment [54]. Novel agents or treatments are urgently needed to improve the outcome for the large number of patients who relapse after receiving the currently available breast cancer therapies, since the existing therapies are no longer effective in these patients [55]. In the present study, the **SCP 1** was designed and synthesized to examine the effects on viability and proliferation of MCF7 human breast cancer cell line. Different concentrations of the **SCP 1** was prepared and dissolved in complete RPMI-1640 media with 10% serum. Cell inhibition rates were determined by MTT assay. The results revealed that **SCP 1** inhibited the growth of MCF7 cells in a dose-dependent manner, Fig. 10. Growth inhibition of 50% (IC₅₀) is calculated as the **SCP 1** concentrations, which caused a 50% reduction in cell proliferation during the drug

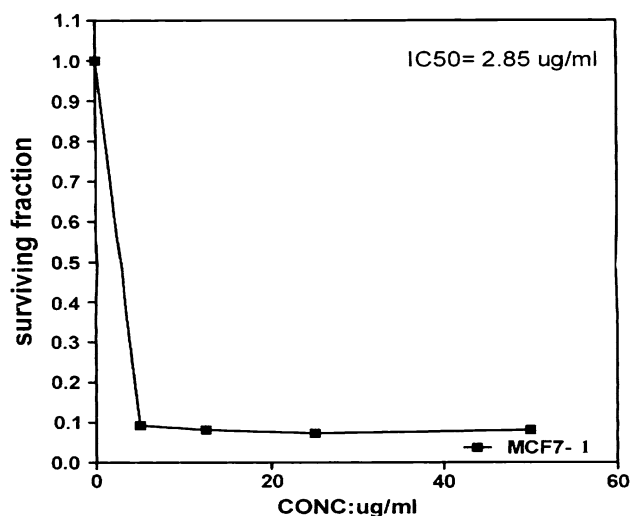


Fig. 10 In vitro cytotoxicity of the **SCP 1** against MCF7 human breast cancer cell line, using different concentrations of the **SCP 1**. Each data point is an average of three independent experiments and expressed as $M \pm SD$

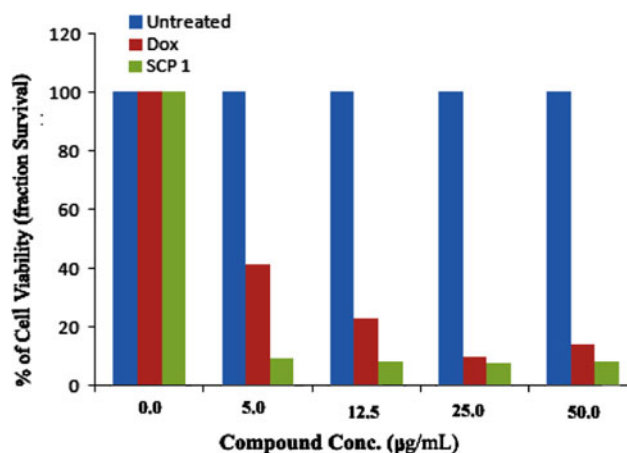


Fig. 11 In vitro cytotoxicity of the **SCP 1** and Doxorubicin (DOX) drug against MCF7 human breast cancer cell line, using different concentrations of the **SCP 1** or DOX. Untreated cells were used as mock. Each data point is an average of three independent experiments and expressed as $M \pm SD$

incubation. The mean IC₅₀ is the concentration of drug that reduces cell growth by 50% under the experimental conditions and is the average with SEM from at least three independent determinations. The **SCP 1** showed an inhibition of cell viability giving an IC₅₀ value of 2.85 µg/ml. The cytotoxicity of the **SCP 1** was found to be more effective towards MCF7 cell lines than that of the drug DOX which gives IC₅₀ value of 4.35 µg/ml. These results indicating that, the tested **SCP 1** is more cytotoxic against cancer cells compared to the drug DOX. Taken together, the tested **SCP 1** at a concentration of IC₅₀ value decreased cell viability of MCF7 cell line compared to the control group, Fig. 11.

4 Supplementary Data

CCDC 814954 contains the supplementary crystallographic data for **1**. These data can be obtained free of charge via <http://www.ccdc.cam.ac.uk/conts/retrieving.html>, or from the Cambridge Crystallographic Data Centre, 12 Union Road, Cambridge CB2 1EZ, UK; fax: (+44) 1223-336-033; or e-mail: deposit@ccdc.cam.ac.uk

References

- B.A. Maynard, R.E. Sykora, J.T. Maguec, A.E.V. Gorden, *Chem. Commun.* **46**, 4944 (2010)
- J. Larionova, Y. Guari, C. Blanc, P. Dieudonne, A. Tokarev, C. Guerin, *Langmuir* **25**, 1138 (2009)
- Z. Su, K. Cai, J. Fan, S.S. Chen, M.S. Chen, W.Y. Sun, *Cryst. Eng. Commun.* **12**, 100 (2010)

4. L.F. Ma, L.Y. Wang, M. Du, S.R. Batton, *Inorg. Chem.* **49**, 365 (2010)
5. S.E.H. Etaiw, A.S. Sultan, M.M. El-Bendary, *J. Organomet. Chem.* **696**, 1668 (2011)
6. M. Ohba, H. Okawa, *Coord. Chem. Rev.* **198**, 313 (2000)
7. L.M. Toma, R. Lescouezec, D. Cangussu, R. Llusar, J. Mata, S. Spey, J.A. Thomas, F. Lloret, M. Julve, *Inorg. Chem. Commun.* **8**, 382 (2005)
8. S.E.H. Etaiw, S.A. Amer, M.M. El-Bendary, *J. Mater. Sci.* **45**, 1307 (2010)
9. S.E.H. Etaiw, S.A. Amer, M.M. El-Bendary, *Polyhedron* **28**, 2385 (2009)
10. S.E.H. Etaiw, M.M. El-Bendary, *J. Inorg. Organomet. Polym.* **20**, 739 (2010)
11. A.N. Ley, L.E. Dunaway, T.P. Brewster, M.D. Dembo, T.D. Harris, F. Baril-Robert, X. Li, H.H. Patterson, R.D. Pike, *Chem. Commun.* **46**, 4565 (2010)
12. S.V. Wegner, H. Arslan, M. Sunbul, J. Yin, C. He, *J. Am. Chem. Soc.* **132**, 2567 (2010)
13. E. Colacio, R. Kivekas, F. Lloret, M. Sunberg, J.S. Varela, M. Bardaji, A. Laguna, *Inorg. Chem.* **41**, 5141 (2002)
14. L.-L. Li, L.-L. Liu, A.-X. Zheng, Y.-J. Chang, M. Dai, Z.-G. Ren, H.-X. Lia, J.-P. Lang, *Dalton Trans.* **39**, 7659 (2010)
15. L. Hou, W.-J. Shi, Y.-Y. Wang, B. Liu, W.-H. Huang, Q.-Z. Shi, *CrystEngComm* **12**, 4365 (2010)
16. X. He, C.Z. Lu, C.D. Wu, L.J. Chen, *Eur. J. Inorg. Chem.* **12**, 2491 (2006)
17. S.E.H. Etaiw, A.S. Badr El-din, *J. Inorg. Organomet. Polym.* **21**, 110 (2011)
18. C. Kappestein, U. Schubert, *Chem. Commun.* 1116 (1980)
19. K. Wasielewski, R. Mattes, *Z. Naturforsch. B Chem. Sci.* **47**, 1795 (1992)
20. P.G. Sammes, G. Yahioglu, *Chem. Soc. Rev.* **23**, 327 (1994)
21. J.-P. Sauvage, C.O. Dietrich-Buchecker (ed.), *Molecular catenanes, rotaxanes and knots. A journey through the world of molecular topology* (Wiley-VCH, Weinheim, Germany, 1999)
22. S. Bonnet, J.P. Collin, M. Koizumi, P. Mobian, J.P. Sauvage, *Adv. Mater.* **18**, 1239 (2006)
23. K. Hayashi, H. Akutsu, H. Ozaki, H. Sawai, *Chem. Commun.* 1386 (2004)
24. J.W. Eastes, W.M. Burgess, *J. Am. Chem. Soc.* **64**, 1187 (1942)
25. M. Wicholas, T. Wolford, *Inorg. Chem.* **13**, 316 (1974)
26. M. Dunaj-Jurčo, I. Potočňák, J. Cívik, M. Kabešová, *Acta Cryst.* **C49**, 1479 (1993)
27. H. Masuda, K. Machida, M. Munakata, S. Kitagawa, H. Shimono, *J. Chem. Soc. Dalton Trans.* 1907 (1988)
28. L. Stamp, T. Dieck, *Inorg. Chim. Acta* **129**, 107 (1987)
29. T. Pintauer, *J. Organomet. Chem.* **691**, 3948 (2006)
30. R.H. Holm, P. Kennepohl, E.I. Solomon, *Chem. Rev.* **96**, 2239 (1996)
31. M. Kondo, Y. Shibuya, K. Nabari, M. Miyazawa, S. Yasue, K. Maeda, F. Uchida, *Inorg. Chem. Commun.* **10**, 1311 (2007)
32. J. Costamagna, F. Caruso, J. Vargas, V. Manriquez, *Inorg. Chim. Acta* **267**, 151 (1998)
33. J.R.B. Gomes, M.A.V. Ribeiro da Silva, *Inorg. Chem. Commun.* **6**, 149 (2003)
34. L. Gutierrez, G. Alzuet, J. Borrás, M. Liu-González, F. Sanz, A. Castiñeiras, *Polyhedron* **20**, 703 (2001)
35. V. Broughton, G. Bernardinelli, A.F. Williams, *Inorg. Chim. Acta* **275–276**, 279 (1998)
36. K.R. Dunbar, R.A. Heintz, *Prog. Inorg. Chem.* **45**, 283 (1997)
37. K.-Y. Ho, W.-Y. Yu, K.-K. Cheung, C.-M. Che, *Chem. Commun.* 2101 (1998)
38. X.-C. Huang, S.-L. Zheng, J. -P. Zhang, X.-M. Chen, *Eur. J. Inorg. Chem.* 1024 (2004)
39. A. Spalletti, G. Cruciani, U. Mazzucato, *J. Mol. Struct.* **612**, 339 (2002)
40. H.H. Jalfé, M. Orechin, *Theory and Applications of Ultraviolet Spectroscopy*, 5th edn. (Wiley, New York, 1970)
41. N. Armaroli, L.D. Cola, V. Balzani, J.-P. Sauvage, C. Dietrich-Buchecker, J.-M. Kern, *J. Chem. Soc. Faraday Trans.* **88**, 553 (1992)
42. B.N. Bandyopadhyay, A. Harriman, *J. Chem. Soc. Faraday Trans.* **1**, 73 (1977)
43. G. M. Badger, I. S. Walker, *J. Chem. Soc.* 122 (1956)
44. K. Yamamoto, T. Takemura, H. Baba, *Bull. Chem. Soc. Jpn.* **51**, 729 (1978). and references therein
45. M.J. Lim, C.A. Murray, T.A. Tronic, K.E. deKrafft, A.N. Ley, J.C. deButts, R.D. Pike, H. Lu, H.H. Patterson, *Inorg. Chem.* **47**, 6931 (2008)
46. C.A. Bayse, T.P. Brewster, R.D. Pike, *Inorg. Chem.* **48**, 174 (2009)
47. J.M. Monteagudo, A. Durán, I. San Martín, M. Aguirre, *Appl. Catal. B Environ.* **95**, 120 (2010)
48. L. Dapeng, G. Jiuhui, *J. Environ. Sci.* **21**, 713 (2009)
49. J.M. Campos-Martin, G. Blanco-Brieva, J.L.G. Fierro, *Angew. Chem. Int. Ed.* **45**, 6962 (2006)
50. Y. Lu, M. Tonigod, B. Breidenkötter, D. Volkmer, J. Hitzbleck, G. Langstein, *Z. Anorg. Allg. Chem.* **634**, 2411 (2008)
51. C. Flox, S. Ammar, C. Arias, E. Brillas, A. Vargas-Zaval, R. Abdehdi, *Appl. Catal. B Environ.* **67**, 93 (2006)
52. J. De Laat, T.G. Le, *Appl. Catal. B Environ.* **66**, 137 (2006)
53. G. Chelucci, R.P. Thummel, *Chem. Rev.* **102**, 3129 (2002)
54. A.S. Sultan, J. Xie, M.J. LeBaron, L.E. Ealley, M.T. Nevalainen, H. Rui, *Oncogene* **24**, 746 (2005)
55. A.S. Sultan, H. Brim, Z.A. Sherif, *Cancer Sci.* **2**, 272 (2008)